

Photoluminescence properties of silicon nanocrystals interacting with gold nanoparticles via exciton-plasmon coupling

Karsten Potrick and Friedrich Huisken*

*Laboratory Astrophysics Group of the Max Planck Institute for Astronomy at the Friedrich Schiller University Jena,
Institute of Solid State Physics, Helmholtzweg 3, D-07743 Jena, Germany*

(Received 4 November 2014; revised manuscript received 16 February 2015; published 18 March 2015)

The photoluminescence (PL) properties of silicon nanocrystals (Si NCs) deposited on gold nanostructures have been studied regarding PL intensity and lifetime. In contrast to most investigations, which attempt to optimize the overlap between the plasmon resonance and the Si NCs' PL band, we chose much smaller gold nanoparticles to achieve an improved exciton-plasmon coupling. PL enhancements of up to 20 were observed near the plasmon resonance. In the maximum of the PL band at 710 nm, we determined a PL enhancement of ~ 4 while the average PL lifetime was found to increase from 45 to 66 μs . The experimental observations were successfully explained with a model invoking bidirectional energy transfer between excitonic and plasmonic states, being operative in addition to the normal exciton recombination rate enhancement.

DOI: [10.1103/PhysRevB.91.125306](https://doi.org/10.1103/PhysRevB.91.125306)

PACS number(s): 78.67.Bf, 71.35.Gg, 73.21.La, 78.47.jd

I. INTRODUCTION

Silicon nanocrystals (Si NCs) are an important representative of indirect semiconductor quantum dots and a basic building block of promising nanotechnological devices. For a comprehensive review of their properties and applications in nanoelectronics, photonics, photovoltaics, and nanobiotechnology, the reader is referred to the recent book edited by Pavesi and Turan [1].

Si NCs show efficient photoluminescence (PL) in the visible to near infrared range when excited by UV radiation. The PL may originate from radiative recombination of electron-hole pairs (excitons) created by the UV photons [2], or it may arise from luminescent defect centers [3]. Both mechanisms compete with each other and can be active within the same nanocrystal [4]. The origin of the PL depends very much on the method of synthesis and on the size of the Si NCs. Chemical synthesis routes, in particular if they include surface functionalization, and small nanocrystal sizes favor the creation of luminescent defect centers. In contrast, for Si NCs produced by CO_2 laser-induced pyrolysis of silane in a flow reactor and gently passivated via oxidation in air, it could be shown that their PL was predominantly caused by radiative exciton recombination [2,5,6]. As this PL is governed by quantum confinement its characteristic properties (PL wavelength, exciton lifetime, and quantum efficiency) are functions of the NCs' size and can thus be tuned [7]. For some applications, further size-independent tuning is desirable. One way to achieve this is to exploit the interaction between the excitons of the Si NCs and the plasmons of metal nanostructures. In the past, such systems have mainly been investigated with the goal to obtain higher PL yields.

For Si NCs in a SiO_2 matrix, the highest reported PL intensity enhancement in the presence of nanoscale Ag island arrays is sevenfold [8]. Gold nanostructures have been demonstrated to increase the brightness of Si NCs by a factor of 5 [9]. In most studies, such enhancements of the PL intensity were accompanied by an increase of the emission

rate [9–11]. For porous silicon, a decay rate increase together with a quenching of the PL intensity was observed in the presence of a semicontinuous gold film [12]. In contrast, Bassu *et al.* [13] found for a system with gold nanoparticles a PL intensity enhancement that was associated with a reduced recombination rate. In this paper, we report on a study of the PL properties of Si NCs on top of small ($d = 14.4$ nm) gold nanoparticles. The improved exciton-plasmon coupling results in an 3.9-fold PL enhancement at 710 nm and a lifetime retardation from 45 to 66 μs .

II. EXPERIMENT

Colloidal gold nanoparticles (Au NPs) from a PELCO AFM calibration kit having an average diameter of (14.4 ± 0.9) nm were drop-casted on a fused silica (FS) window. Atomic force microscopy (AFM) measurements reveal that, after the evaporation of the solvent, the drop-casted Au NPs agglomerate on the FS window and randomly arrange themselves to form agglomerates of varying size and shape that are composed of up to two monolayers of Au NPs, as shown in Fig. 1. The small separation between individual particles causes a shift of the plasmon resonance that will be discussed in Sec. III.

About one-half of the Au NP layer was covered by a thin layer of Si NCs with an average diameter of (4.3 ± 0.9) nm employing the cluster beam deposition technique [14]. For this purpose, the Si NCs were synthesized by CO_2 laser-induced pyrolysis of silane in a gas flow reactor and expanded into a vacuum to form a freely propagating beam of Si NCs [5,6]. To prevent all Au NPs from being covered by the Si NCs, part of the Au NP layer was protected by a glass cover slip. The deposition time of 36 min resulted in a Si NC layer thickness of 83 nm, with a porosity of approximately 78% [15].

For the PL excitation of the Si NCs, a continuous-wave (cw) diode laser (Coherent, model Cube 405-50C) operating at $\lambda = 406$ nm was utilized (spot size: 0.5 mm; irradiance: 240 mW cm^{-2}) to measure steady-state PL spectra and the temporal response of the PL intensity upon switching on and off the excitation source. The switching was achieved by means of a digitally modulated periodic square-wave

*friedrich.huisken@uni-jena.de; <http://www.astrolab.uni-jena.de>

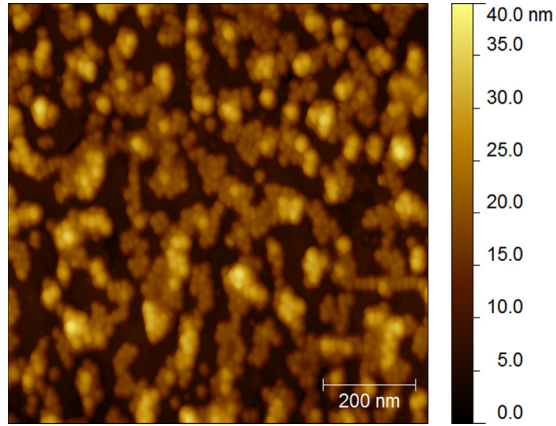


FIG. 1. (Color online) AFM image measured on a $900 \times 900 \text{ nm}^2$ large sample area of the FS window covered with Au NPs only. Agglomerates consisting of one or two monolayers are formed.

signal. Decay measurements under pulsed excitation of $\sim 10 \text{ ns}$ duration were carried out with a quadrupled Nd:YAG laser. The luminescence setup was arranged in the so-called reflection at 45° geometry [16], where the detection was perpendicular to the sample surface and the incident angle of the excitation beam was 45° . To enable measurements in the frequency and time domains, the emitted PL photons were collected with a lens attached to an optical fiber and analyzed with either a miniature spectrometer (Ocean Optics, model QE65000) or a 30 cm scanning monochromator (McPherson, model 218) equipped with a photomultiplier tube (Burle Electron Tubes, model C31034), respectively. Transmission measurements were performed with a spectrophotometer (Jasco, model V-670).

III. RESULTS AND ANALYSIS

In Fig. 2, we present in panels (a) and (b) photographs of the interesting part of the sample seen under an optical microscope when it is illuminated by a normal lamp and an ultraviolet (UV) lamp ($\lambda = 254 \text{ nm}$), respectively. The Au NPs are located on the left of the circular border, originating from the drop-casting procedure. The Si NCs were deposited on the entire area to the right of the vertical line marking the edge of the cover slip. Hence the photos show three different areas of nanoparticle coverage, which are from left to right: Au NPs only, Si NCs on top of Au NPs, and Si NCs only. Under UV illumination, the Au NPs show a weak blue PL while the Si NCs on Au NPs reveal rather strong orange-red PL and the Si NCs on bare FS appear weakly red because their major PL response is in the infrared (IR).

The PL spectra shown in Fig. 3(a) were acquired 6 months after sample preparation. Therefore, the passivation of the Si NCs by natural oxidation in air was already completed [2]. All PL spectra shown were corrected for the response of the entire optical system. The PL spectrum of bare Si NCs deposited directly on the FS window (unaffected by Au NPs) is given by the black curve. Their broad PL band extending from the red to the near-IR is caused by the radiative recombination of excitons in Si NCs [7] and peaks at 819 nm . For the Si NCs deposited on Au NPs, the PL band (light gray or brown curve)

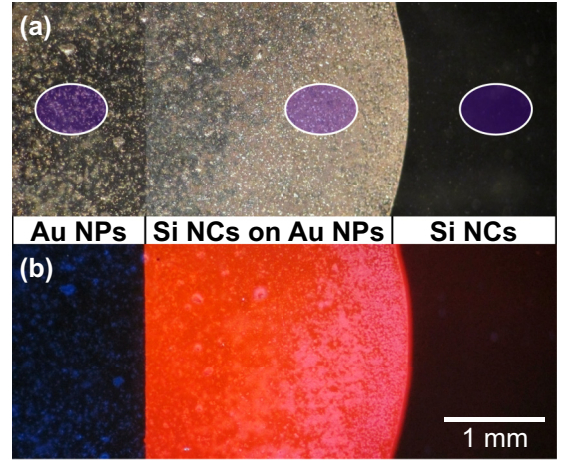


FIG. 2. (Color online) Photographs of the sample seen under an optical microscope and illuminated by a normal lamp (a) and an UV lamp with $\lambda = 254 \text{ nm}$ (b). To view the enhanced red PL of the Si NCs on top of the Au NP layer, the reader is referred to the online version of this article. The three positions, where the PL was measured, are marked by ellipses representing the spots illuminated by the laser.

is blueshifted and has its maximum at 711 nm . Moreover, its intensity in the visible is considerably increased as was already shown in Fig. 2. The bare Au NPs give rise to a blue PL band (dark blue dashed curve) peaking at 480 nm . Of course, this band also contributes to the PL measured when both Au NPs and Si NCs are present. The small narrow peak at 406 nm showing up in all spectra is caused by the scattered laser light leaking through the 405 nm long-wave pass filter.

The spectral dependence of the Si NCs' PL enhancement is plotted in Fig. 3(b) by the light gray (or brown) curve. It is obtained as the ratio of the two solid curves of Fig. 3(a) (Si NCs

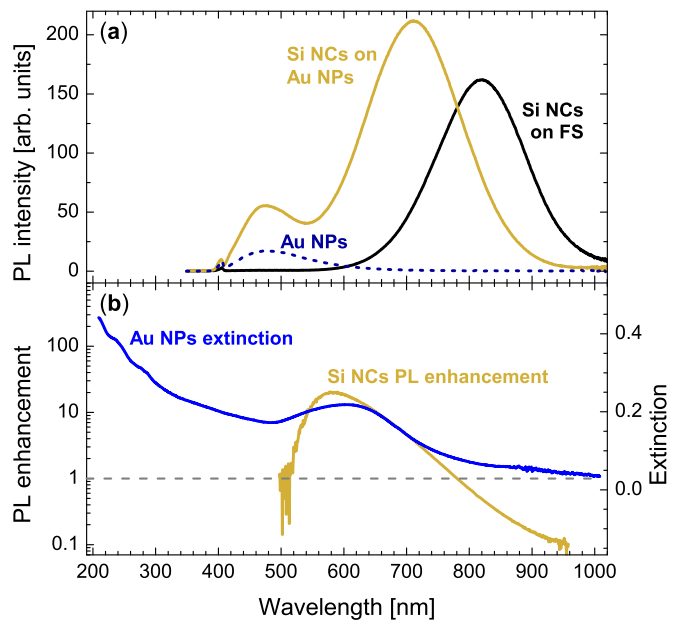


FIG. 3. (Color online) (a) PL spectra of Si NCs deposited on FS and on Au NPs as well as of Au NPs drop-casted on FS. (b) PL enhancement for the Si NCs together with the extinction of Au NPs.

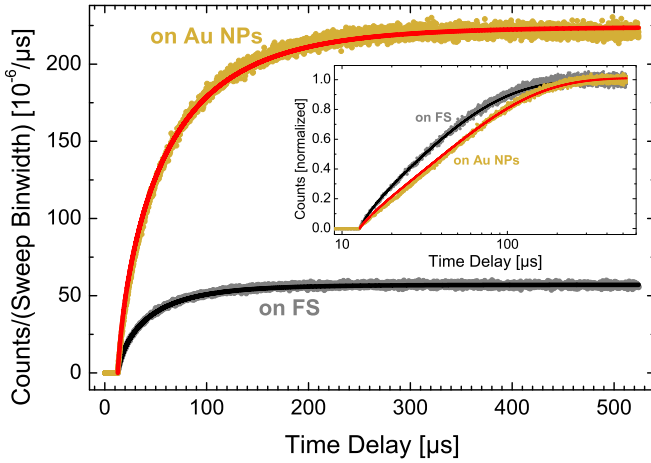


FIG. 4. (Color online) Photoluminescence response of Si NCs deposited on FS and on Au NPs measured at $\lambda = 710$ nm upon switching on the cw laser. Fits to the measured data (dots) are shown as solid lines. For a better visualization of the slower response in the presence of Au NPs, the inset shows the same data on a normalized scale.

on Au NPs / Si NCs on FS) after having subtracted the properly scaled blue band arising from the Au NPs. An up-scaling of the blue Au PL band was necessary, in order to account for the higher density of Au NPs at the position where the Si NC emission was measured (see Fig. 2). As it was demonstrated that the PL emission of Si NCs on FS is isotropic [17] and because the Au NPs are randomly distributed on the substrate and do not reveal any symmetry, periodicity, or preferred orientation, we do not expect that the PL enhancement is anisotropic. PL measurements carried out from the backside of the sample, i.e., for the light emitted through the Au NP layer and the substrate, revealed practically the same PL enhancement values for the entire wavelength range proving that the presence of the Au NPs does not significantly alter the ratio of the fluorescence emitted into the forward or backward direction. Also shown in Fig. 3(b) is the extinction of Au NPs drop-casted on FS. Although the Au NPs have a relatively narrow size distribution, their plasmon resonance at 605 nm is rather broad and redshifted with respect to their theoretical plasmon resonance at 518 nm [18]. This shift is due to a near-field plasmon coupling between the irregularly arranged Au NPs.

The coincidence of the Au NPs' plasmon resonance with the PL enhancement for the Si NCs is a strong indication for plasmon-enhanced luminescence [8,9]. For an emitter coupled to the plasmon modes of a metal sphere, an enhanced PL intensity is associated with increased recombination or absorption rates. An increase in one or both of these rates would result in a faster temporal response of the PL to a sudden optical excitation [19]. However, we clearly observed a slower response upon switching on the diode laser when gold NPs are involved. The corresponding data is presented in Fig. 4. To demonstrate the strong signal enhancement, we have plotted in the main frame the measured signals in absolute intensities. On the other hand, the slower response of the Si NCs on Au NPs is best seen if the curves are normalized as shown in the inset of the same figure.

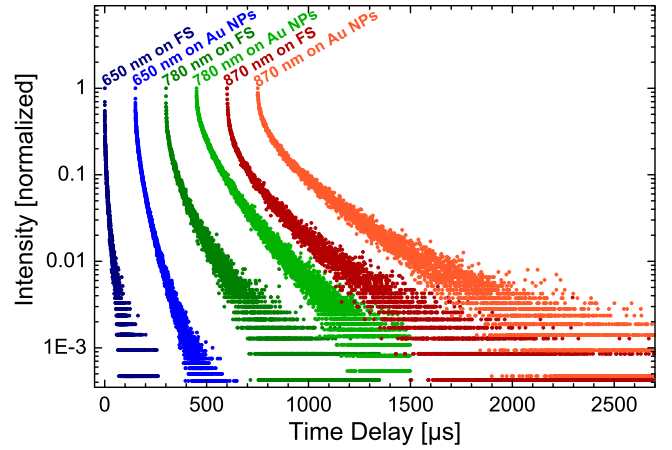


FIG. 5. (Color online) Photoluminescence decay curves at three different emission wavelengths. For a clearer presentation, the starting point of each curve has been shifted by $150 \mu\text{s}$ towards larger times.

Similarly, decay measurements after pulsed excitation at 266 nm from a quadrupled Nd:YAG laser that we have carried out at various wavelengths consistently reveal a slower decay if the Si NCs are residing on Au NPs. These decay curves are shown in Fig. 5 on a normalized scale and with shifted starting points for a better visualization.

On the one hand, the spectral PL enhancement presented in Fig. 3(b) suggests an exciton-plasmon interplay between the Si NCs and the Au NPs as the origin, but on the other hand, the time-resolved measurements revealing a slower response to switching the excitation laser on or off apparently are in contradiction to a normal interaction [8–12]. Therefore, we extended the model to include a bidirectional energy transfer between exciton and plasmon.

A schematic representation of the model is given in Fig. 6. The Si NCs in the ground state S_0 with population n_0 absorb the incoming laser light, are excited above the band gap (HOMO-LUMO gap), and relax on a ps-time scale to the lowest excited state S_1 [20]. As this relaxation is much faster than the processes governing the PL time dependence we can neglect it and may consider just a direct excitation from S_0 to S_1 with an excitation rate k_{01} . The portion of Si NCs carrying one exciton is n_1 . Since the utilized excitation laser irradiance

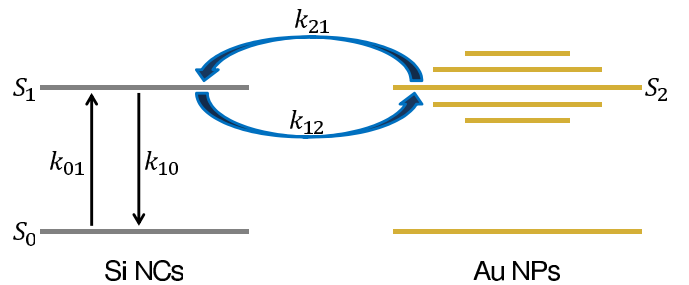


FIG. 6. (Color online) Simplified diagram illustrating relevant energy levels, populations, and transition rates. In the given example, the exciton of the Si NC is in resonance with the plasmon of the Au NP. For larger (smaller) Si NCs of our sample, the exciton energy will be lower (higher) while the plasmon energy remains always the same.

is low and the nonradiative Auger recombination time is faster than 1 ns [21,22], the existence of Si NCs with two and more excitons can be neglected. The exciton recombination rate k_{10} includes all radiative and nonradiative paths (subscripts “r” and “nr,” respectively), i.e.,

$$k_{10} = k_r^{\text{Si}} + k_{\text{nr}}^{\text{Si}} + k_r^{\text{Au}} + k_{\text{nr}}^{\text{Au}} = f_r k_r^{\text{Si}} + k_{\text{nr}}^{\text{Si}} + k_{\text{nr}}^{\text{Au}}, \quad (1)$$

where the superscripts Si and Au refer to the rates intrinsic to the Si NCs and those induced by the presence of the Au NPs, respectively. An increased optical mode density causes an additional radiative deexcitation path (k_r^{Au}) that can also be described by the effective radiative rate enhancement f_r . Due to dissipation in and electronic energy transfer to Au NPs, nonradiative deexcitation paths ($k_{\text{nr}}^{\text{Au}}$) arise too. The bidirectional energy transfer by dipole-dipole Coulomb interaction is described by the transfer rates k_{12} and k_{21} . Direct excitation of plasmons can be neglected, due to the nonresonant excitation wavelength, and energy dissipation from the plasmonic state S_2 is implicitly included in $k_{\text{nr}}^{\text{Au}}$, because k_{12} and k_{21} are much higher than $k_{\text{nr}}^{\text{Au}}$, as our analysis will show.

The following system of state-filling equations gives a mathematical description of our model:

$$\begin{aligned} \dot{n}_0 &= -n_0 k_{01} + n_1 k_{10}, \\ \dot{n}_1 &= n_0 k_{01} - n_1 (k_{10} + k_{12}) + n_2 k_{21}, \\ \dot{n}_2 &= n_1 k_{12} - n_2 k_{21}. \end{aligned} \quad (2)$$

The excitation rate is given by $k_{01} = f_{\text{exc}} k_{01}^{\text{Si}}$, where k_{01}^{Si} is the excitation rate for Si NCs without Au NPs and the factor f_{exc} describes the modification of the effective absorption cross section by the presence of Au NPs.

For response (superscript “R”) measurements upon switching on the excitation laser, all Si NCs are initially in their ground state, and Eq. (2) can be solved analytically. The solution can be written as

$$I_{\text{PL}}^{\text{R}}(t) = a_{\text{ss}} (1 - a_s^{\text{R}} e^{-k_s^{\text{R}} t} - a_f^{\text{R}} e^{-k_f^{\text{R}} t}), \quad (3)$$

with the steady-state PL intensity

$$a_{\text{ss}} = N_{\text{Si}} \frac{k_{01} f_r k_r^{\text{Si}} k_{21}}{k_{10} k_{21} + k_{01} k_1} \quad (4)$$

and the relative intensities

$$a_s^{\text{R}} = \frac{1}{2k_{\text{ia}}^{\text{R}}} \left(k_{\text{ia}}^{\text{R}} + k_t - k_{10} - \frac{k_{01}}{k_{21}} (k_t + k_{12}) \right), \quad (5a)$$

$$a_f^{\text{R}} = \frac{1}{2k_{\text{ia}}^{\text{R}}} \left(k_{\text{ia}}^{\text{R}} - k_t + k_{10} + \frac{k_{01}}{k_{21}} (k_t + k_{12}) \right) \quad (5b)$$

of a slow and a fast component (subscripts “s” and “f,” respectively). The corresponding effective rates are

$$k_s^{\text{R}} = \frac{1}{2} (k_{01} + k_{10} + k_t - k_{\text{ia}}^{\text{R}}), \quad (6a)$$

$$k_f^{\text{R}} = \frac{1}{2} (k_{01} + k_{10} + k_t + k_{\text{ia}}^{\text{R}}), \quad (6b)$$

with the abbreviations

$$k_{\text{ia}}^{\text{R}} = \sqrt{(k_{01} + k_{10} + k_t)^2 - 4(k_{10} k_{21} + k_{01} k_1)} \quad (7)$$

and k_t for the sum of the transfer rates, $k_{12} + k_{21}$.

To determine the exciton recombination rate k_{10} , quasi-steady-state decay measurements were performed. The results

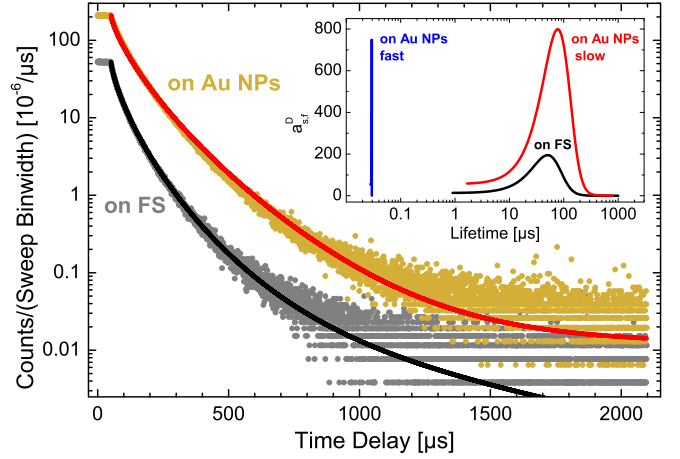


FIG. 7. (Color online) Photoluminescence decay of Si NCs deposited on FS and on Au NPs at a wavelength of $\lambda = 710$ nm. The inset shows the lifetime distributions corresponding to the fits shown as solid lines in the main frame. Note the fast component of the bimodal lifetime distribution of Si NCs on Au NPs, which peaks around 30 ns.

upon switching off the excitation laser obtained for Si NCs on fused silica and on Au NPs are shown in Fig. 7. For decay measurements, k_{01} is zero, and the solution of the set of rate equations [Eq. (2)] with the steady-state signal as initial condition becomes

$$I_{\text{PL}}^{\text{D}}(t) = a_{\text{ss}} (a_s^{\text{D}} e^{-k_s^{\text{D}} t} + a_f^{\text{D}} e^{-k_f^{\text{D}} t}). \quad (8)$$

For calculating the amplitudes (a_s^{D} and a_f^{D}) and the rates (k_s^{D} , k_f^{D} , and k_{ia}^{D}), Eqs. (5)–(7) can be used when the superscript “R” is replaced by “D” and k_{01} set to zero.

The presented model describes how the response of a single Si NC with PL lifetime $\tau_{\text{PL}}^{\text{Si}} = 1/(k_r^{\text{Si}} + k_{\text{nr}}^{\text{Si}})$ upon switching on and off the excitation laser is modified by the presence of the Au NP layer. However, the PL of a Si NC ensemble exhibits a multiexponential decay behavior associated with a lifetime distribution of nonvanishing width [23]. Therefore, we first derived the PL lifetime distribution for the Si NCs on FS emitting at a wavelength of $\lambda = 710$ nm from the decay curve in Fig. 7. For this purpose, the measured gray data points were fitted by applying the maximum entropy algorithm developed by Skilling and Bryan [24] (see black solid line in Fig. 7 and the resulting distribution with an average time constant of $45 \mu\text{s}$ in the inset therein). With the quantum efficiency $\eta_{\text{PL}}^{\text{Si}}$, the associated radiative and nonradiative rates are specified by $k_r^{\text{Si}} = \eta_{\text{PL}}^{\text{Si}}/\tau_{\text{PL}}^{\text{Si}}$ and $k_{\text{nr}}^{\text{Si}} = (1 - \eta_{\text{PL}}^{\text{Si}})/\tau_{\text{PL}}^{\text{Si}}$, respectively. Knowing the PL lifetime, we can utilize the response measurement for Si NCs on FS (gray data points in Fig. 4) to determine the excitation rate k_{01}^{Si} , which is the difference between the decay and response rates [19]. The fit to the measured data (black solid line in Fig. 4) yields a value of 3.4 kHz for k_{01}^{Si} . Now the model can be used for every single PL lifetime, and the resulting lifetime distribution for the Si NCs on Au NPs can be calculated for any specific set of model parameters. As, besides the PL lifetimes, this calculation also determines the corresponding intensities, the decay and response curves for the Si NCs on Au NPs are obtained on an absolute scale that represents the change in the

TABLE I. Model parameters with their values and confidence intervals (CI).

| Parameter | Median | 95% CI |
|----------------------|--------|-----------------|
| f_r | 14.5 | (13.1,17.0) |
| f_{exc} | 0.78 | (0.38,0.91) |
| k_{12} (MHz) | 26.0 | (19.3,47.3) |
| k_{21} (MHz) | 7.8 | (5.8,14.6) |
| k_{nr}^{Au} (MHz) | 0.0028 | (0.0017,0.0063) |
| η_{PL}^{Si} (%) | 12.4 | (5.8,14.2) |

total PL intensity emitted at the given wavelength. The entire procedure is implemented into a least square fitting routine [25] that fits the model parameters (f_r , f_{exc} , k_{12} , k_{21} , k_{nr}^{Au} , and η_{PL}) simultaneously to the decay and response measurements for Si NCs on Au NPs on an absolute scale, taking into account the full lifetime distribution derived for Si NCs on fused silica.

The free parameters together with their best-fit values and 95% confidence intervals, determined by bootstrap analysis, are summarized in Table I. The fits to the measured data on Au NPs (in absolute intensities) are shown in Figs. 4 and 7 by the red solid curves while the associated lifetime distributions are presented in the inset of Fig. 7.

IV. DISCUSSION

At first, we would like to emphasize that the apparent shift of the PL band observed in our experiment [see Fig. 3(a)] does not result from a PL shift of the individual Si NCs. The degree of PL enhancement depends on the energy difference between the excited states of the Si NC (the exciton energy) and the Au NP (the plasmon energy). At wavelengths larger than 780 nm, even quenching is observed. The exciton energy of the Si NCs varies over the entire emission band (with $1/\lambda$, where λ is the emission wavelength). Thus Si NCs, which have an exciton energy close to the plasmon resonance, experience a stronger PL enhancement than those with an exciton energy farther away from the plasmon resonance. Hence the overall effect of the exciton-plasmon interaction on the PL band of the Si NCs is an apparent shift to the blue.

For the proper interpretation of the results, it is important to note that, for Si NCs on Au NPs, the PL rates measured in the time domain are not only determined by k_{10} as it is the case for Si NCs on FS. Instead, the population of S_1 probed by these measurements is also affected by a bidirectional energy exchange represented by the transition rates k_{12} and k_{21} . The presence of Au NPs results in a faster transition rate k_{10} because the radiative rate is increased by the factor f_r due to the higher optical mode density and because an additional nonradiative deexcitation path k_{nr}^{Au} has been introduced [see Eq. (1)]. In addition, S_1 is depleted by k_{12} . This causes an initial acceleration of the PL process being described by the fast component (k_f) with an average time constant of 29 ns. However, this fast component only contributes with 0.5% to the total PL intensity emitted at 710 nm. This is due to the facts that k_{12} competes with k_{10} and that S_1 is subsequently refilled with the rate k_{21} . In summary, the interaction processes effectively result in a retardation of the PL, which is characterized by the slow component (k_s) with an average time constant of 66 μ s.

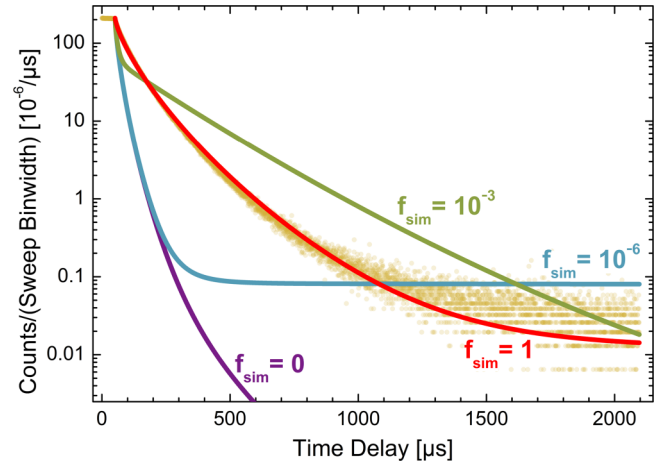


FIG. 8. (Color online) Simulated PL decay of Si NCs on Au NPs at an emission wavelength of 710 nm. The coupling strength was continually reduced by decreasing f_{sim} from one (unchanged coupling strength) to zero (no energy transfer).

We attribute the fact that almost all earlier experiments did not reveal any retardation of the PL to the special plasmonic nanostructure utilized. Instead of relatively large Au nanostructures whose plasmon resonance overlaps with the emission spectrum of the Si NCs, we used arrays of small agglomerated Au NPs that are coupled to each other due to their close proximity and therefore have a redshifted plasmon resonance. For such small spheres, the emitter-plasmon coupling is more efficient than for larger structures. Moreover, the shift of the resonance not only results in a better spectral overlap, but also in a reduction of interband transitions, which are prominent in Au NPs only below 600 nm [26].

To further illustrate the influence of the bidirectional energy transfer on the characteristics of the PL decay (retardation vs acceleration), we calculated the expected PL decay for weaker couplings. For this purpose, we replaced the rates k_{12} and k_{21} by $f_{sim}k_{12}$ and $f_{sim}k_{21}$, respectively. The value of f_{sim} was continually reduced from one (unchanged interaction) to zero (no energy exchange), while all other parameter values were kept unchanged. The results are presented in Fig. 8. It is clearly seen that the PL decay rate gets faster if the energy exchange is reduced, reaching its most extreme value when there is no exchange at all. This is the situation in experiments, where small Si NCs are coupled to large gold nanostructures. Accordingly, in such experiments, the Si NCs on Au exhibit faster decay than Si NCs without gold.

Deviation from the normal exciton-plasmon coupling has already been observed for other nanosystems. Stronger interaction mechanisms have been demonstrated, e.g., for the excitons of CdSe NCs and surface plasmons of a thin Ag film by means of reflection measurements [27] as well as for J-aggregate-Au nanoshell complexes (gold nanoshells covered by an organic semiconductor) via transient absorption spectroscopy [28]. To explain their experimental observations, the authors invoked a coherent coupling mechanism. Although the present rate model describes our measurements very well, it does not provide any evidence whether such coherent coupling is also

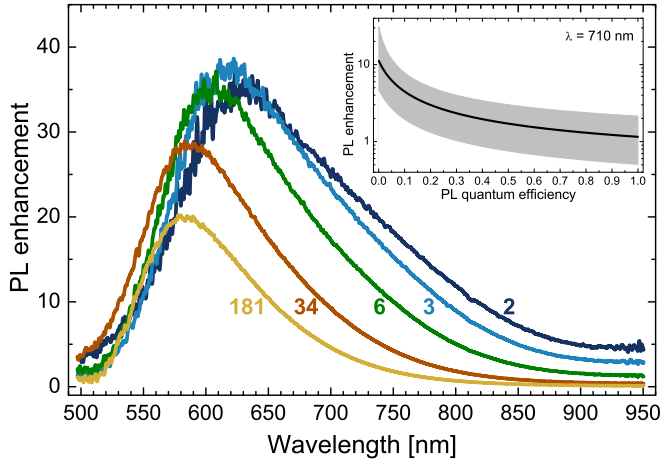


FIG. 9. (Color online) Spectral dependence of the PL enhancement for the given sample as a function of time after synthesis (given in days). The inset shows the dependence of the PL enhancement on the quantum efficiency $\eta_{\text{PL}}^{\text{Si}}$ as predicted by the model. The gray area is determined by the confidence intervals of the model parameters.

effective in our Si NC–Au NP system. Rigorous quantum model calculations would be necessary to answer this question.

The presented model can be used to describe other relations, like the dependence of the PL enhancement on the quantum efficiency $\eta_{\text{PL}}^{\text{Si}}$. For Si NCs synthesized by laser-induced pyrolysis, $\eta_{\text{PL}}^{\text{Si}}$ is a function of the time the sample has aged in air [2]. As a result of the progressive but self-terminating passivation of dangling bonds due to oxidation, the PL quantum efficiency continually increases before it goes into saturation [29]. In Fig. 9, the curve displayed in light gray or brown (denoted by 181), which is the same as the one presented in Fig. 3(b), is compared to the enhancement spectra derived from measurements on the same sample at earlier times. The PL enhancement at a wavelength of $\lambda = 710$ nm decreases continuously within the observation interval. This behavior is in agreement with the dependence of the PL enhancement on the quantum efficiency as predicted by the model, which is shown in the inset of Fig. 9. However, it should be pointed out that, despite the reduction of the PL enhancement with sample age, the absolute intensity emitted increases with time, e.g., by more than a factor of 3 for the time period from 2 to 181 days. As a whole, the sample aging is accompanied by a gradual reduction of the integral PL enhancement and a narrowing of the PL bandwidth. The decreasing effect on the PL enhancement ascribed to the interaction with the gold nanoparticles is consistent with the model of plasmon-induced PL enhancement irrespective of whether bidirectional energy transfer is considered or not.

Up to now, we have only discussed the effect of the plasmon-exciton coupling on the temporal characteristics (response and decay curves) of the PL emission at 710 nm, where the maximum PL intensity ensured a high signal-to-noise level (see Fig. 3). Nevertheless, additional response and decay measurements were carried out at 650, 780, and 850 nm. The experimental data was subjected to the full fitting procedure described before, yielding the complete set of fit parameters (f_r , f_{exc} , k_{12} , k_{21} , $k_{\text{nr}}^{\text{Au}}$, and η_{PL}) also as

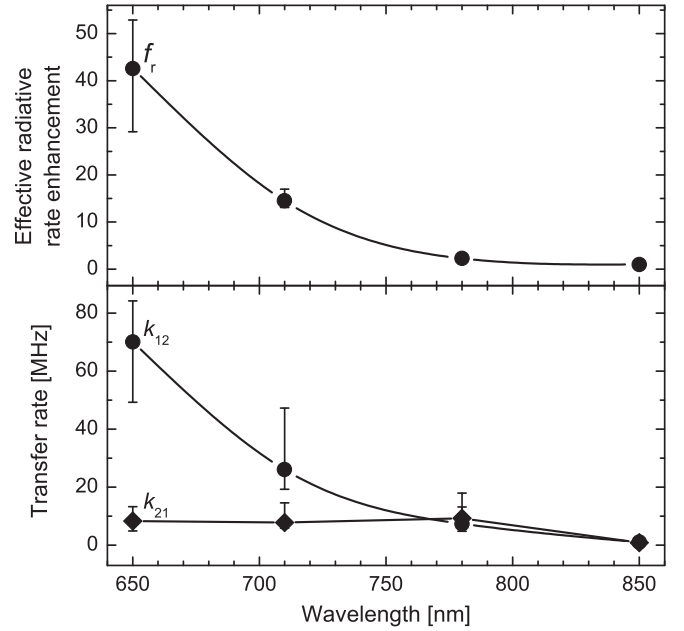


FIG. 10. Effective radiative rate enhancement, f_r , and transfer rates, k_{12} and k_{21} , as a function of the emission wavelength. The curves are drawn to guide the eye.

a function of wavelength. The wavelength dependences of the three most important parameters f_r , k_{12} , and k_{21} are presented in Fig. 10. The effective radiative rate enhancement f_r continuously decreases with increasing separation from the plasmon resonance at 605 nm and is equal to 1 at large separation (e.g., at 850 nm). This behavior is expected and also observed for systems in which bidirectional energy transfer is absent.

The rate for energy transfer from the Si NCs to the Au NPs, k_{12} , is governed by the availability of plasmonic states in the Au NPs at energies equal to the exciton energies of the Si NCs. As the density of plasmonic states decreases with increasing wavelength separation between the Si NCs' emission and the maximum of the plasmon resonance, k_{12} diminishes with increasing PL emission wavelength. The energy transfer rate back to the Si NCs, k_{21} , is small and almost constant over the entire wavelength range. This can be rationalized if one considers that the density of states of the Si NCs at the band gap edge is almost independent of the band gap size and thus the emission wavelength.

As far as the fit parameters are concerned, we can summarize the following. The effective change of the excitation rate, f_{exc} , due to the presence of Au NPs is constant and close to unity, which means that the Au NPs have no effect on the excitation of the Si NCs. The rate for the nonradiative deexcitation path $k_{\text{nr}}^{\text{Au}}$ is found to be very small over the entire wavelength range. Finally, as could be expected, the quantum efficiency η_{PL} is not affected by the Au NPs. Moreover, the wavelength dependence of η_{PL} , showing a maximum around 700 nm, is in good agreement with an earlier study of our laboratory [7].

Finally, it should be emphasized that the strength of the exciton-plasmon coupling depends on the separation between the Si NC and the Au NP. With a layer thickness of 83 nm, we

offer a large range of separations, which includes the optimum separation. Therefore, the measured PL enhancement is the result of an averaging over many separations. If the layer were considerably thicker, the effect would be less pronounced since the Si NCs being too far away would not contribute to the enhancement. As our model does not explicitly take into account the separation dependence it rather describes the average effect of the exciton-plasmon coupling for our specific layer thickness. However, it should be stressed that the Si NCs having the optimum separation contribute most to the PL enhancement. The structural inhomogeneity within the Si NC and Au NP layers is not considered as a disadvantage. Since we average over a large number of configurations, we do not favor a specific constellation, which could be particularly bad or good.

V. CONCLUSIONS

In conjunction with the analysis, our experimental results reveal that the PL properties of Si NCs on Au NPs are governed by a bidirectional energy transfer between excitonic and plasmonic states in addition to the normal exciton

recombination rate enhancement. Such a mechanism may also be effective in other exciton-plasmon systems, leading to an enhancement of the PL intensity with a simultaneous retardation of the PL emission. While all practical applications benefit from the intensity enhancement, the increased PL lifetime may be useful for solar cell design, in biomedicine, for photochemical reactions, and for the realization of Si NC-based lasers. Moreover, the concomitant shift of the emission spectra into the visible may be advantageous for various optoelectronic devices. To further exploit the detailed coupling between Si NCs and Au NPs, the ideal study would be an experiment, in which a single Si NC can be moved with respect to a well-defined cluster of Au NPs with a piezoelectric actuator. However, it should be considered that, due to the slow radiative recombination of excitons in indirect semiconductors, such an experiment will be extremely difficult.

ACKNOWLEDGMENTS

The financial support of the Max Planck Institute for Astronomy in Heidelberg is gratefully acknowledged.

-
- [1] *Silicon Nanocrystals: Fundamentals, Synthesis and Applications*, edited by L. Pavesi and R. Turan (Wiley-VCH, Weinheim, 2010).
 - [2] G. Ledoux, J. Gong, and F. Huysen, *Appl. Phys. Lett.* **79**, 4028 (2001).
 - [3] A. G. Cullis, L. T. Canham, and P. D. J. Calcott, *J. Appl. Phys.* **82**, 909 (1997).
 - [4] T. Schmidt, A. I. Chizhik, A. M. Chizhik, K. Potrick, A. J. Meixner, and F. Huysen, *Phys. Rev. B* **86**, 125302 (2012).
 - [5] G. Ledoux, O. Guillois, D. Porterat, C. Reynaud, F. Huysen, B. Kohn, and V. Paillard, *Phys. Rev. B* **62**, 15942 (2000).
 - [6] F. Huysen, G. Ledoux, O. Guillois, and C. Reynaud, *Adv. Mater.* **14**, 1861 (2002).
 - [7] G. Ledoux, J. Gong, F. Huysen, O. Guillois, and C. Reynaud, *Appl. Phys. Lett.* **80**, 4834 (2002).
 - [8] J. S. Biteen, N. S. Lewis, H. A. Atwater, H. Mertens, and A. Polman, *Appl. Phys. Lett.* **88**, 131109 (2006).
 - [9] J. Goffard, D. Gérard, P. Miska, A.-L. Baudrion, R. Deturche, and J. Plain, *Sci. Rep.* **3**, 2672 (2013).
 - [10] J. L. Biteen, D. Pacifici, N. S. Lewis, and H. A. Atwater, *Nano Lett.* **5**, 1768 (2005).
 - [11] Y. Mochizuki, M. Fujii, S. Hayashi, T. Tsuruoka, and K. Akamatsu, *J. Appl. Phys.* **106**, 013517 (2009).
 - [12] T. Nakamura, B. P. Tiwari, and S. Adachi, *Opt. Express* **20**, 26548 (2012).
 - [13] M. Bassu, M. L. Strambini, G. Barillaro, and F. Fuso, *Appl. Phys. Lett.* **97**, 143113 (2010).
 - [14] F. Huysen, H. Hofmeister, B. Kohn, M. A. Laguna, and V. Paillard, *Appl. Surf. Sci.* **154–155**, 305 (2000).
 - [15] F. Voigt, G. Bauer, and F. Huysen, *J. Appl. Phys.* **106**, 034308 (2009).
 - [16] I. Pelant and J. Valenta, *Luminescence Spectroscopy of Semiconductors* (Oxford University Press, New York, 2012).
 - [17] D. Amans, S. Callard, A. Gagnaire, J. Joseph, F. Huysen, and G. Ledoux, *J. Appl. Phys.* **95**, 5010 (2004).
 - [18] B. K. Juluri, J. Huang, and L. Jensen, “Extinction, scattering and absorption efficiencies of single and multilayer nanoparticles”, <https://nanohub.org/resources/8228>.
 - [19] D. Kovalev, J. Diener, H. Heckler, G. Polisski, N. Künzner, and F. Koch, *Phys. Rev. B* **61**, 4485 (2000).
 - [20] W. D. A. M. de Boer, D. Timmerman, K. Dohnalova, I. N. Yassievich, H. Zhang, W. J. Buma, and T. Gregorkiewicz, *Nat. Nanotechnol.* **5**, 878 (2010).
 - [21] C. Delerue, M. Lannoo, G. Allan, E. Martin, I. Mihalcescu, J. C. Vial, R. Romestain, F. Muller, and A. Bsiesy, *Phys. Rev. Lett.* **75**, 2228 (1995).
 - [22] M. C. Beard, K. P. Knutsen, P. Yu, J. M. Luther, Q. Song, W. K. Metzger, R. J. Ellingson, and A. J. Nozik, *Nano Lett.* **7**, 2506 (2007).
 - [23] C. Delerue, G. Allan, C. Reynaud, O. Guillois, G. Ledoux, and F. Huysen, *Phys. Rev. B* **73**, 235318 (2006).
 - [24] J. Skilling and R. K. Bryan, *Mon. Not. R. Astron. Soc.* **211**, 111 (1984).
 - [25] Mathematica, Version 9.0, Wolfram Research, Inc., Champaign, IL, 2012.
 - [26] H. Mertens, A. F. Koenderink, and A. Polman, *Phys. Rev. B* **76**, 115123 (2007).
 - [27] D. E. Gómez, K. C. Vernon, P. Mulvaney, and T. J. Davis, *Nano Lett.* **10**, 274 (2010).
 - [28] N. T. Fofang, N. K. Grady, Z. Fan, A. O. Govorov, and N. J. Halas, *Nano Lett.* **11**, 1556 (2011).
 - [29] K. Potrick, T. Schmidt, S. Bubltz, C. Mühligh, W. Paa, and F. Huysen, *Appl. Phys. Lett.* **98**, 083111 (2011).